Spinodal instabilities of baryon-rich quark matter in heavy ion collisions

Feng Li and Che Ming Ko

Phys. Rev. C **95**, 055203 — Published 9 May 2017

DOI: 10.1103/PhysRevC.95.055203

Spinodal instabilities of baryon-rich quark matter in heavy ion collisions

Feng Li[1,*] and Che Ming Ko[1,†]

[1] *Cyclotron Institute and Department of Physics and Astronomy, Texas A&M University, College Station, TX 77843-3366, USA*

Using the test-particle method to solve the transport equation derived from the Nambu-Jona-Lasino (NJL) model, we study how phase separation occurs in an expanding quark matter like that in a heavy ion collision. To test our method, we first investigate the growth rates of unstable modes of quark matter in a static cubic box and find them to agree with the analytical results that were previously obtained using the linear response theory. In this case, we also study the higher-order scaled density moments in the quark matter, which have values of one for a uniform density distribution or a distribution where the non-zero density regions all have same value, and they are found to increase with time and saturate at values significantly larger than one after the phase separation. The skewness of the quark number event-by-event distribution in a small sub-volume of the system is also found to increase, but this feature disappears if the sub-volume is large. For the expanding quark matter, two cases are considered with one using a blast-wave model for the initial conditions and the other using initial conditions from a mulple-phase transport (AMPT) model. In both cases, we find the expansion of the quark matter is slowed down by the presence of a first-order phase transition. Also, density clumps appear in the system and the momentum distribution of partons becomes anisotropic, which can be characterized by large scaled density moments and non-vanishing anisotropic elliptic and quadrupolar flows, respectively. The large density fluctuations further lead to an enhancement in the dilepton yield. In the case with the AMPT initial conditions, the presence of a first-order phase transition also results in a narrower distribution of partons in rapidity. These effects of density fluctuations can be regarded as possible signals for a first-order phase transition that occurs in the baryon-rich quark matter formed in relativistic heavy ion collisions.

I. INTRODUCTION

Studying the properties of baryon-rich quark-gluon plasma (QGP) is the main focus of the beam energy scan (BES) experiments [1–5] at the Relativistic Heavy Ion Collider (RHIC) as well as at the future Facility for Antiproton and Ion Research (FAIR). These experiments are expected to shed light on whether the phase transition from the baryon-rich QGP to the hadronic matter is a first-order one and the location of the critical end point in the QCD phase diagram if the phase transition is first-order. To help understand what could happen in a baryon-rich QGP, we have recently used the Polyakov-Nambu-Jona-Lasinia (PNJL) model to study its spinodal instability [6]. We have found via the linear response theory that the spinodal boundary in the temperature and density plane of the QCD phase diagram shrinks with increasing wave number of the unstable mode and is also reduced in the absence of the Polyakov loop. In the small wave number or long wavelength limit, the spinodal boundary coincides with that determined from the isothermal spinodal instability in the thermodynamic approach. We have further found that the quark vector interaction suppresses unstable modes of all wave numbers. For the wave number dependence of the growth rate of an unstable mode, it initially increases with the wave number but decreases when the wave number is large. For the collisional effect from quark scattering, we have included it via the linearized Boltzmann equation and found it to decrease the growth rates of unstable modes of all wave numbers. In the present study, we continue the above work by investigating how unstable modes would grow if one goes beyond the linear response or small amplitude limit. This is carried out by using the transport equation derived from the NJL model [7–9] to study the time evolution of density fluctuations in a confined as well as in an expanding quark matter. Specifically, we study the time evolution of higher-order density moments in the quark matter, the distribution of quark number in a sub-volume of the quark matter, the quark momentum anisotropy, and dilepton production rate from quark-antiquark annihilation. As shown below, some of these observables could serve as signatures for a first-order phase transition of the baryon-rich quark matter produced in heavy ion collisions. We note that there have already been a number of studies on the spinodal instability of quark matter in heavy ion collisions based on either schematic models or the hydrodynamic approach [10–14]. These studies are, however, for quark matter near thermal equilibrium and are thus different from the present study based on the transport approach that can take into account the non-equilibrium effect.

The paper is organized as follows: In the next section, we give a brief review on the NJL model and the transport equations based on its Lagrangian. The transport equations are solved by the test-particle method in Section III to study both the short and long time behavior of the spinodal instability of quark matter in a periodic

*Electronic address: lifengphysics@gamil.com
†Electronic address: ko@comp.tamu.edu

box. The same method is applied in Section IV to an expanding quark matter to study how density fluctuations are affected by the expansion of the system as in heavy ion collisions. Finally, a summary is given in Section V. In the Appendix, we describe in detail the effect due to the finite grid size used in the numerical calculations on the growth rate of unstable modes.

II. THE NJL MODEL AND THE TRANSPORT MODEL

The NJL Lagrangian containing only the scalar interaction for three quark flavors has the form [15]:

$$\mathcal{L}^S_{NJL} = \bar{q}(i\not{\partial} - m_0)q + \frac{G_S}{2}\sum_{a=0}^{8}\left[(\bar{q}\lambda^a q)^2 + (\bar{q}i\gamma_5\lambda^a q)^2\right] -K\left[\det{}_f\Big(\bar{q}(1+\gamma_5)q\Big) + \det{}_f\Big(\bar{q}(1-\gamma_5)q\Big)\right], \quad (1)$$

where $q = (u, d, s)^T$, $m_0 = \mathrm{diag}(m_{0u}, m_{0d}, m_{0s})$ and λ^a are the Gell-Mann matrices for $a = 1, 2\cdots 8$, with λ^0 being the identity matrix multiplied by $\sqrt{2/3}$. The Lagrangian preserves $U(1) \times SU(N_f)_L \times SU(N_f)_R$ symmetry but breaks the axial symmetry, which is broken in QCD by the axial anomaly, by the Kobayashi-Masakawa-t'Hooft (KMT) interaction given by the last term in Eq. (1) [16]. The $\det_f$ in this term denotes the determinant in the flavor space [17], that is

$$\det{}_f(\bar{q}\Gamma q) = \sum_{i,j,k}\varepsilon_{ijk}(\bar{u}\Gamma q_i)(\bar{d}\Gamma q_j)(\bar{s}\Gamma q_k), \quad (2)$$

where Γ denotes either a Dirac gamma or the identity matrix. The determinantal term is responsible for obtaining the correct splitting in the masses of η and η' mesons.

Because the NJL model is not renormalizable, a regularization scheme is required to remove infinities in the momentum integrations. In this study, we assume that all interactions are among quarks of 3-momenta with magnitudes below the cutoff momentum Λ. Taking $\Lambda = 0.6023$ GeV, the values of the scalar coupling G_S and the KMT interaction K can be determined from fitting the pion mass, the kaon mass, and the pion decay constant, and their values are $G_S\Lambda^2 = 3.67$, and $K\Lambda^5 = 12.36$ if the current quark masses are taken to be $m_{0u} = m_{0d} = 3.6$ and $m_{0s} = 87$ MeV [18].

A flavor-singlet vector interaction can be added to the NJL Lagrangian as follows:

$$\mathcal{L}^V_{NJL} = -G_V(\bar{q}\gamma^\mu q)^2, \quad (3)$$

where the coupling strength G_V is assumed to be independent of the temperature T and the net quark chemical potential μ. The value of G_V affects the order of quark matter phase transition. If G_V is large, the first-order phase transition induced by the attractive scalar interaction could disappear [6]. In the present study, we treat it as a parameter to change the equation of state of quark matter.

For describing the quark matter produced in a heavy ion collision, we use the Boltzmann (or transport) equations that can be derived from the NJL Lagrangian in terms of the non-equilibrium Green's functions for quarks and antiqaurks [7], and they are:

$$\partial_{X^0} f_a(X,\mathbf{p}) + \frac{p^{i\pm}}{E_{\mathbf{p}^\pm}}\partial_{X^i} f_a(X,\mathbf{p}) -\partial_{X^i}V^S_a(X)\frac{m_a}{E_{\mathbf{p}^\pm}}\partial_{p_i} f_a(X,\mathbf{p}) \mp \partial_{X^i}V^V_0(X)\partial_{p_i} f_a(X,\mathbf{p}) \mp\partial_{X^i}V^V_j(X)\frac{p^{j\pm}}{E_{\mathbf{p}^\pm}}\partial_{p_i} f_a(X,\mathbf{p}) = \mathcal{C}[f_a], \quad (4)$$

where $f_a(X,\mathbf{p})$ is the phase-space distribution function of quarks or antiquarks of flavor a. In the above, $\mathbf{p}^\pm \equiv \mathbf{p} \pm \mathbf{V}^V$ is the kinetic momentum with the subscript $+$ referring to quarks and $-$ referring to antiquarks, $V^V_\mu = -2G_V\sum_a\langle\bar{q}\gamma_\mu q\rangle_a$ is the vector potential, and $m_a = m_{0a} - V^S_a$ is the effective quark mass with $V^S_a = 2G_S\langle\bar{q}q\rangle_a + 2K\langle\bar{q}q\rangle_b\langle\bar{q}q\rangle_c$ being the scalar potential with $a \neq b \neq c$.

The right hand side of Eq.(4),

$$\mathcal{C}[f_a] \equiv \sum_{bcd}\frac{1}{1+\delta_{ab}}\int\frac{d^3\mathbf{p}_b}{(2\pi)^3 2E_b}\frac{d^3\mathbf{p}_c}{(2\pi)^3 2E_c}\frac{d^3\mathbf{p}_d}{(2\pi)^3 2E_d}\frac{(2\pi)^4}{2E_a}\delta^4(p_a+p_b-p_c-p_d) \times|\mathcal{M}_{ab}|^2\left[f_c f_d(1-f_a)(1-f_b) - f_a f_b(1-f_c)(1-f_d)\right], \quad (5)$$

is the collisional term that describes the scatterings among quarks and antiquarks, with the subscripts a, b, c, and d denoting not only the flavor but also the spin, color, and baryon charge (quark or anti-quark) of a parton. The above equation can be solved using the test particle method [19] by expressing the distribution function in terms of the density of test particles, whose equations of motions are determined by the left hand side of

Eq.(4), and they are

$$\dot{\mathbf{x}} = \frac{\mathbf{p}^{\pm}}{E_{\mathbf{p}^{\pm}}}, \quad (6)$$

$$\dot{\mathbf{p}} = \nabla V^S(\mathbf{x})\frac{m}{E_{\mathbf{p}^{\pm}}} \pm \nabla V_0^V(\mathbf{x}) \pm \nabla V_j^V(\mathbf{x})\frac{p^{j\pm}}{E_{\mathbf{p}^{\pm}}}. \quad (7)$$

The second equation in the above can also be written as

$$\dot{\mathbf{p}}^{\pm} = \nabla V^S(\mathbf{x})\frac{m}{E_{\mathbf{p}}} \mp \dot{\mathbf{x}} \times \mathbf{B} \pm \mathbf{E}, \quad (8)$$

where $\mathbf{B} = \nabla \times \mathbf{V}^V$ is the strong magnetic field and $\mathbf{E} = \partial_t \mathbf{V}^V + \nabla V^S$ is the strong electric field.

Besides mean fields, test particles are also affected by collisions, which can be treated geometrically by generalizing the method of Ref. [20] to use the particle scattering cross section σ in the quark matter frame to check whether the impact parameter between two colliding particles is smaller than $\sqrt{\sigma/\pi}$ and if they pass through each other at the next time step during the evolution of the system. For two particles of masses m_A and m_B, momenta $\mathbf{p}_A$ and $\mathbf{p}_B$, and energies E_A and E_B, this cross section is related to the cross section in their center-of-mass frame $\sigma_{\rm CM}(\sqrt{s})$ with $s = (p_A + p_B)^2$ being the square of their invariant mass, which is the one used in Ref. [20], by

$$\sigma = \sigma_{\rm CM}(\sqrt{s})\frac{\sqrt{(s-(m_A+m_B)^2)(s-(m_A-m_B)^2)}}{2E_AE_B|\mathbf{v}_A - \mathbf{v}_B|}. \quad (9)$$

In the above, $\mathbf{v}_A = \mathbf{p}_A/E_A$ and $\mathbf{v}_B = \mathbf{p}_B/E_B$ are the velocities of the two particles. The 3-momenta of the two particles after the scattering are taken to be isotropic in their center-of-mass frame. Because of the high quark baryon chemical potential considered in the present study, the Pauli blocking effect on scatterings is also included by checking the available phase space for the final states [20]. We have checked that the above treatment of parton scattering reproduces the expected scattering rate evaluated via direct numerical integrations.

III. QUARK MATTER IN A BOX

This section serves as a bridge between the studies of the spinodal instabilities in the small and large amplitude limits. Although the case of small amplitude has already been discussed in Ref. [6], we can develop an intuitive picture for how an initial sinusoidal fluctuation in a baryon-rich quark matter grows during the early stage of its time evolution from solving the Boltzmann equation in the test particle method as discussed in the previous section. For the large amplitude case, which also includes the growth of instabilities during the late stage, solving the Boltzamnn equation allows us to follow the whole phase separation process to see how dense clusters develop inside a box of initially uniform quark matter and finally lead to the formation of large scale structures. It also provides the possibility to find the appropriate observables to characterize these structures.

A. Small amplitude density fluctuations

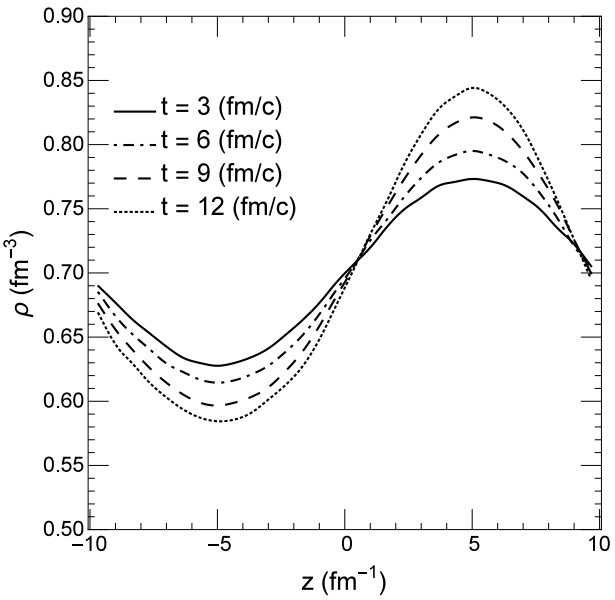

FIG. 1: Time evolution of an unstable density mode of wave number $k = 0.31$ fm^{-1}.

We consider a quark matter that is confined in a cubic box with periodic boundary conditions. The system is prepared by distributing many test particles inside the box according to the density of the system with their momenta given by the Fermi-Dirac distribution at certain temperature. We then study the growth of density fluctuations from an initial distribution with density and temperature corresponding to that inside the spinodal region. Results obtained from solving the Boltzmann equation by following the classical motions of these test particles are compared with those obtained from the linear response theory in Ref. [6]. Specifically, we introduce an initial density fluctuation that has a sinusoidal oscillation in the z direction, $\rho_{\rm ini} = \rho_0(1 + 0.1\sin(2\pi z/L))$, where ρ_0 is the average initial density and L is the length of the box with $L = 10,\ 20,\ 30,\ 40,\ 50$ fm corresponding to wave numbers $k = 0.63,\ 0.31,\ 0.21,\ 0.16,\ 0.13$ fm^{-1}, respectively. As an example, Fig. 1 shows how the amplitude of the sinusoidal oscillation, which is obtained by averaging over 100 events with each event having 1000 test particles for one physical particle, grows with time in the case of $L = 20$ fm, the average density $\rho_0 = 0.7$ fm^{-3}, and an initial temperature $T = 45$ MeV. Since the amplitude of density fluctuation at early times is expected to grow exponentially, it can be approximated by a hyperbolic

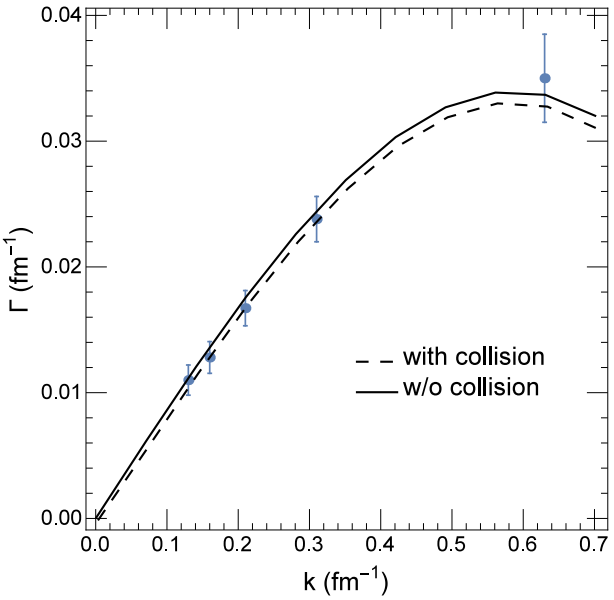

FIG. 2: Growth rates extracted from numerically solving the Boltzmann equation for unstable modes of wave numbers 0.13, 0.16, 0.21, 0.31, and 0.63 fm^{-1} for quark matter of density $\rho = 0.7$ fm^{-3} and temperature $T = 45$ MeV. Analytical results from the linearized Boltzmann equation of Ref. [6] are shown by solid and dashed curves for the cases with and without the collision term, respectively.

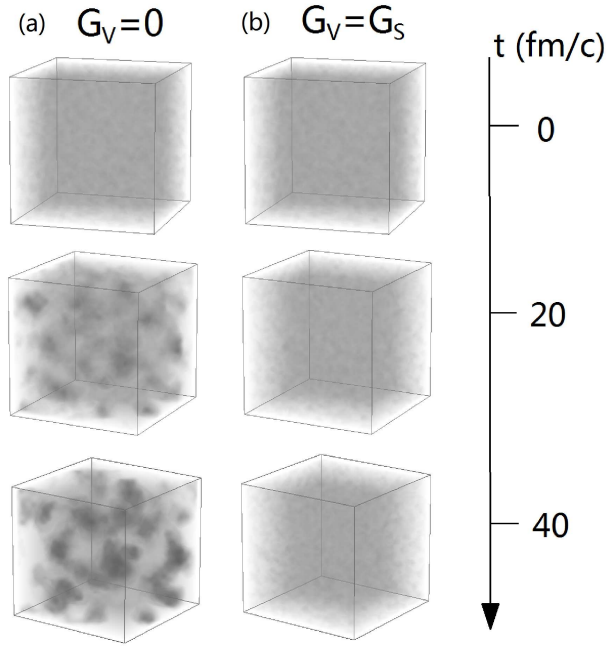

FIG. 3: Time evolution of density distribution for a single event in a quark matter of temperature $T = 20$ MeV and net quark density $n_q = 0.5$ fm^{-3} for the cases of $G_V = 0$ (left column) and $G_V = G_S$ (right column).

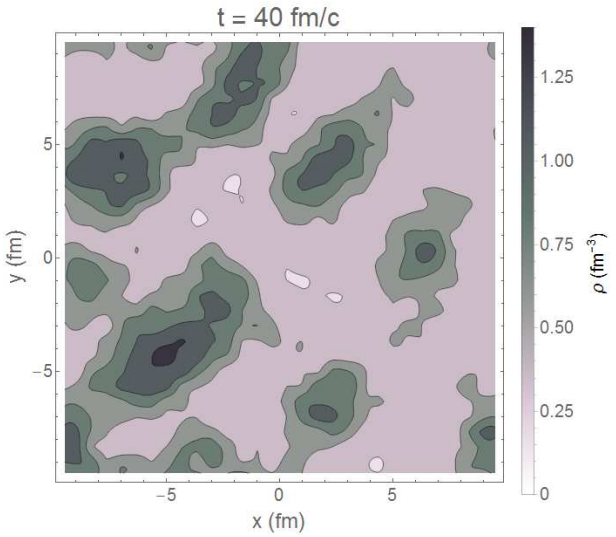

FIG. 4: Cross sectional view of density distribution for a single event on the $z = 0$ plane at $t = 40$ fm/c for the case $G_V = 0$ with a first-order phase transition.

cosine function of time, i.e.,

$$\delta\rho(t) = \delta\rho_0 \cosh(\Gamma_k t), \tag{10}$$

where Γ_k is the growth rate and can be extracted directly from the numerical results, and they are shown in Fig. 2 by filled circles, where the error bars indicate the uncertainty in fitting $\delta\rho(t)$ by Eq. (10). They are seen to agree very well with those obtained from an analytical calculation based on the linearized Boltzmann equation [6] after including the finite grid size effect as described in the Appendix, shown by the solid and dashed lines for the cases with and without the collision term in the Boltzmann equation, respectively.

B. Large amplitude density fluctuations

To study how density fluctuations emerge and grow, we compare results from two calculations based on the same initial conditions but with and without the spinodal instability in the equation of state. This is achieved by introducing a vector interaction in the NJL model, which is known to move the state of a quark matter from inside the spinodal region to the outside if its strength is sufficiently large [6]. For example, for a quark matter of temperature $T_0 = 20$ MeV and net quark density $\rho_0 = 0.5$ fm^{-3}, the spinodal region disappears if the vector coupling G_V has the same value as the scalar coupling G_S, although the state of the quark matter is well inside the spinodal instability region for $G_V = 0$.

Figure 3 shows the time evolution of the density distribution in a box of size $20\times20\times20$ fm^3 for the two cases of $G_V = 0$ (left column) and $G_V = G_S$ (right column) for a single event, with the darker color denoting the high density regions and the lighter color denoting the low

density regions. Although the system is initially uniform in space, some dense spots are present due to statistical fluctuations as a result of finite number of test particles used in the calculation. In the case of $G_V = G_S$ without a first-order phase transition or spinodal instability, the density distribution in the box remains unchanged with time as shown in the right column. This changes dramatically, however, for the case of $G_V = 0$. Due to the spinodal instability, the initial dense spots act like "seeds", which create several small low pressure regions that attract nearby partons and lead to the formation of many clusters at $t = 20$ fm/c. These clusters further grow in size by connecting with each other and form stable large structures at $t = 40$ fm/c, when the system clearly separates into two phases of matter with one of high density and the other of low density.

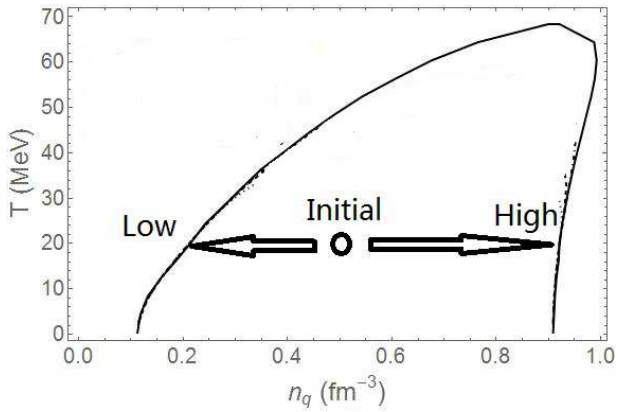

FIG. 5: Demonstration of the phase separation in the phase diagram.

A clearer picture can be obtained by taking a cross sectional view on the $z = 0$ plane as shown by the density distribution contours in Fig. 4. The two phases are now distinguishable with the dilute phase having a density of about 0.25 fm^{-3} and the dense phase having a density of about 1.0 fm^{-3}. According to the phase diagram in Fig. 5, the initial location of the system is indicated by the open circle inside the spinodal region. During the phase separation, the location of most part of the system moves towards the left boundary of the spinodal instability region that has a density of about 0.2 fm^{-3}, while that of the small part of the system moves towards the right boundary of the spinodal instability region that has a density of about 0.9 fm^{-3}, consistent with the picture shown by the density evolution.

As the large scale structure forms, we expect the density-density correlation $\overline{\rho(r)\rho(0)}$ to get stronger and the correlation length to become larger. This is indeed the case as shown in Fig. 6, where it is seen that both the amplitude of the correlation function and the correlation length determined from the average over 1000 events increases with time.

The density fluctuations can also be quantified by the

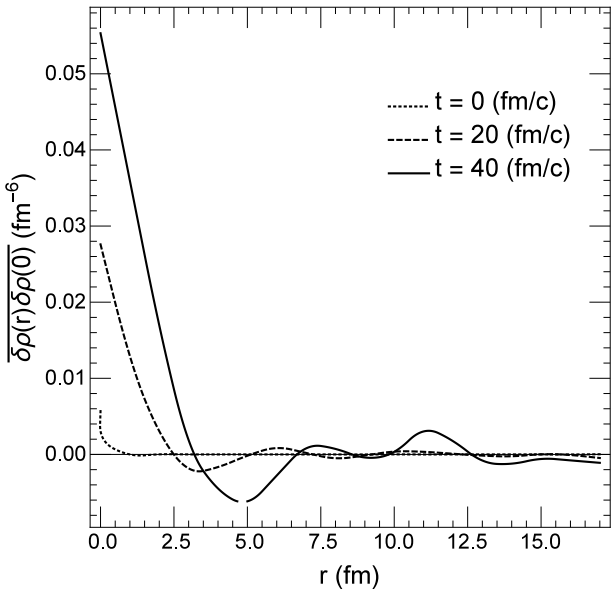

FIG. 6: Time evolution of the density-density correlation function, averaged over 1000 events, in a quark matter of temperature $T = 20$ MeV and average net quark density $n_q = 0.5$ fm^{-3} inside the spinodal region.

scaled density moments $\langle\rho^N\rangle/\langle\rho\rangle^N$ [21], where

$$\langle\rho^N\rangle \equiv \frac{\int d^3\mathbf{r}\rho(\mathbf{r})^{N+1}}{\int d^3\mathbf{r}\rho(\mathbf{r})}. \tag{11}$$

This quantity is scale invariant since its value remains unchanged under a scale transformation $\mathbf{r} \to \lambda\mathbf{r}$, where λ can be any positive number. The scaled density moments are all equal to one for a uniform density distribution or a distribution where the non-zero density regions all have same value but become greater than one as the density fluctuations grow. In Fig. 7, we show by dotted, dashed, and solid lines the event averaged scaled density moments for $N = 2$, 4 and 6, respectively. Our results show that the scaled moments increase during the phase separation and reach their saturated values at about $t = 40$ fm/c, when the phase separation almost ends. Also, moments with larger N increase faster and saturate at larger values. The final saturation values can be estimated as follows. For a system of an initial density ρ_0 that separates into two phases of density ρ_1 and ρ_2 with volumes V_1 and V_2, respectively, the scaled density moments are then

$$\frac{\langle\rho^N\rangle}{\langle\rho\rangle^N} = \frac{\rho_1^{N+1}V_1 + \rho_2^{N+1}V_2}{\left(\rho_1^2V_1 + \rho_2^2V_2\right)^N / \left(\rho_1V_1 + \rho_2V_2\right)^{N-1}}. \tag{12}$$

Using the condition of particle number conservation

$$\rho_1V_1 + \rho_2V_2 = \rho_0(V_1 + V_2), \tag{13}$$

the scaled density moments after the phase separation is

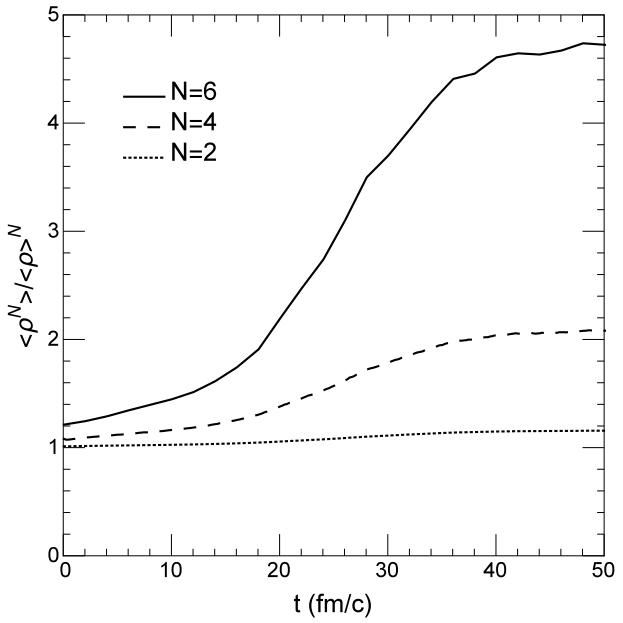

FIG. 7: Time evolution of the scaled density moments, obtained by averaging over 1000 events, in a quark matter of temperature $T = 20$ MeV and average net quark density $n_q = 0.5$ fm^{-3} inside the spinodal region.

thus

$$\frac{\langle\rho^N\rangle}{\langle\rho\rangle^N} = \frac{[\rho_1^{N+1}(\rho_2-\rho_0)+\rho_2^{N+1}(\rho_0-\rho_1)][\rho_0(\rho_2-\rho_1)]^{N-1}}{[\rho_1^2(\rho_2-\rho_0)+\rho_2^2(\rho_0-\rho_1)]^N}. \tag{14}$$

For our case of $\rho_0 = 0.5$ fm^{-3}, $\rho_1 \approx 0.25$ fm^{-3}, and $\rho_2 \approx 1.0$ fm^{-3}, we have $\langle\rho^2\rangle/\langle\rho\rangle^2 \approx 1.22$,$\langle\rho^4\rangle/\langle\rho\rangle^4 \approx 2.11$, and $\langle\rho^6\rangle/\langle\rho\rangle^6 \approx 3.75$, which are close to the final saturation values shown in Fig. 7.

Other quantities of interest are the skewness and kurtosis of the particle multiplicity distribution, which were proposed as possible signals for the critical phenomena [22] and have been studied in the beam energy scan experiments at RHIC [1, 2]. They are defined as follows:

$$\text{skewness} \equiv \frac{\langle\delta N_q^3\rangle}{\langle\delta N_q^2\rangle^{3/2}},$$
$$\text{kurtosis} \equiv \frac{\langle\delta N_q^4\rangle}{\langle\delta N_q^2\rangle^2} - 3. \tag{15}$$

Both quantities characterize how far an event-by-event multiplicity distribution deviates from a normal distribution. A positive skewness means a long tail on the right side of the distribution, i.e., most events have the net quark number below the mean value, while some events have an extreme high net quark number. A positive kurtosis implies a sharper peak than the peak in a normal distribution, while a negative kurtosis corresponds to a flatter one. Theoretical calculations based on the grand canonical picture predict that both quantities diverge with the correlation length when a system approaches its critical point [22], with the kurtosis diverging faster than the skewness. Therefore, they have been suggested as the signals for the existence of a critical end point in the QCD phase diagram.

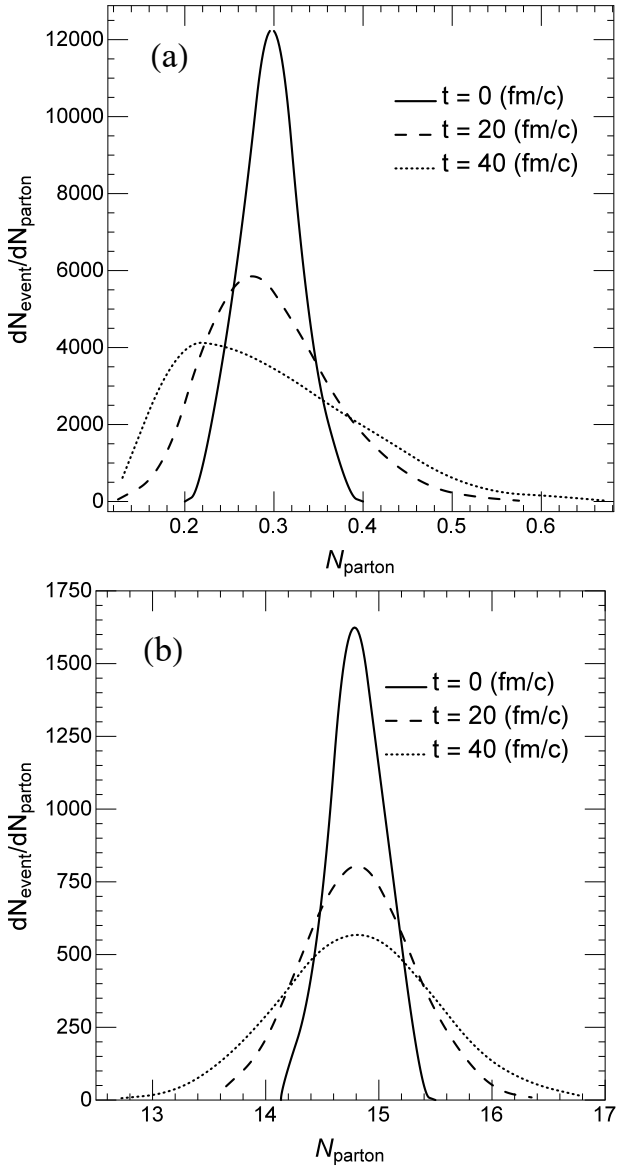

FIG. 8: Time evolution of the event-by-event distribution of the number of quarks in a sub-volume of size 0.6 fm^3 (upper window) and 30 fm^3 (lower window) for a quark matter of temperature $T = 20$ MeV and average net quark density $n_q = 0.5$ fm^{-3} inside the spinodal region. The total number of events is 1000.

To be consistent with the grand canonical picture, we consider quarks in a sub-volume of the box in our study, such as its central cell, and treat the remaining part as the reservoir. When the system is initially inside the spinodal instability region, quarks in the reservoir can sometimes move into the sub-volume, but in most of the times quarks would leave from the sub-volume to the reservoir. The number of quarks inside this sub-volume thus varies

drastically from event to event, leading to large values for the skewness and kurtosis in its event-by-event distribution. In Figs. 8, we show the event-by-event distribution of the number of quarks in the central cell from 1000 events at $t = 0$, 20, and 40 fm/c by the solid, dashed and dotted lines, respectively, for the two cases of sub-volume of size 0.6 fm^3 (upper window) and 30 fm^3 (lower window). The upper window of Fig. 8 clearly shows that the distribution for the small sub-volume becomes asymmetric as time increases, starting with an initial skewness of 0.11 and increasing to 0.60 at 20 fm/c and 0.75 at 40 fm/c. This feature is absent in the lower window of Fig. 8 for the larger sub-volume, where the distribution remains essentially symmetric with increasing time, with the skewness changing slowly from -0.001 (t=0) to 0.086 (t=20 fm/c) and 0.132 (t=40 fm/c), and there is no apparent increase or decrease in the kurtosis. We note that the event-by-event fluctuation shown in Fig. 8 is smooth because of the use of test particles. Even for the small sub-volume of 0.6 fm^3, there are about 300 test particles inside this volume.

The event-by-event parton number fluctuation in the small sub-volumes is, however, not directly observable in heavy ion collisions. What has been measured is the event-by-event net charge or net proton number fluctuation for particles in certain momentum bin [4, 5]. How the latter is related to the number fluctuation in certain spatial volume is not understood and needs to be studied.

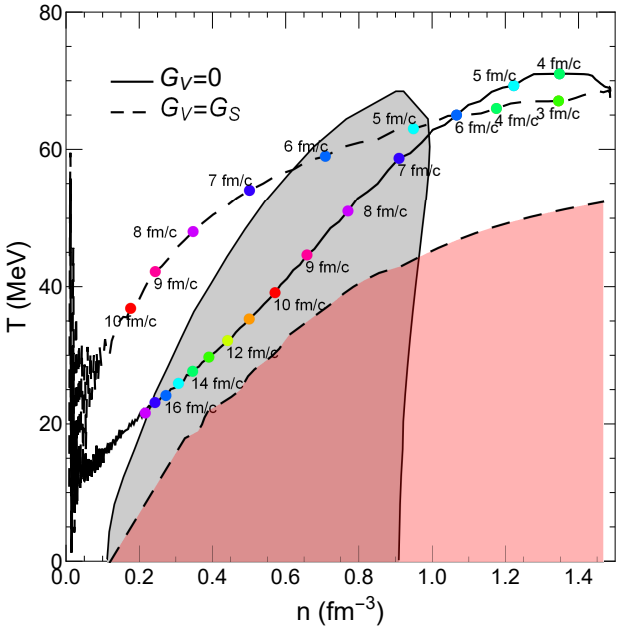

FIG. 9: (Color online). Phase trajectory of the central cell of an expanding quark matter obtained by averaging over 100 events for the two cases with (solid line) and without (dashed line) a first-order phase transition using the blast wave initial conditions. The spinodal region in the case of $G_V = 0$ is shown by the gray color, and it disappears for $G_V = G_S$. The region where quark matter can be bound in the case of $G_V = 0$ is shown by red color.

IV. EXPANDING QUARK MATTER

A. Blast wave initial conditions

To study how large density fluctuations due to the spinodal instability as a result of a first-order phase transition obtained from the box calculation in the previous section are affected by the expansion of the system as in a heavy ion collision, we carry out a dynamical calculation using the transport model that includes parton scatterings besides the mean-field potentials described in Section II. For the initial parton distributions, their positions are taken to follow a spherical Wood-Saxon form:

$$\rho(r) = \frac{\rho_0}{1 + \exp((r - R)/a)} \tag{16}$$

with a radius $R = 5$ fm and a surface thickness parameter $a = 0.5$ fm, similar to that expected from a central Au+Au collisions. The momenta of these partons are again taken to be that of a Fermi-Dirac distribution at certain temperature. Calculations using 1000 test particles for one physical particle are then carried out with two different equations of state with and without a first-order phase transition, which can be realized by adjusting the coupling strength for the vector interaction.

To see how the expanding system goes into the spinodal region in the QCD phase diagram, we first study by averaging over 100 events the time evolution of the temperature and net quark density in the central volume of 42.875 fm^3 that has an initial density $\rho_0 = 1.5$ fm^3 and temperature $T = 70$ MeV, and trace its phase trajectory as shown in Fig. 9 for the two cases with (solid line) and without (dashed line) a phase transition. Although the quark matter described by the transport model may not always be in perfect thermal equilibrium, we approximate its temperature by that of an equilibrated one that has the same energy density and net quark density in the NJL model. As expected, the quark matter with a first-order phase transition (solid curve) enters the spinodal instability region, which is shown by the gray color, at about 6.5 fm/c and leaves the region at about 17.4 fm/c after spending about 10 fm/c inside this region. How the central density decreases with time is shown by the solid line in Fig. 10, which is seen to decrease slower than in the case without a first-order phase transition shown by the dashed line obtained with $G_V = G_S$.

The density fluctuations can be seen from the density distribution for a single event on a plane such as the one at $z = 0$ shown in Fig. 11. The upper window shows the density distribution at $t = 20$ fm/c for the case with a first-order phase transition, while the lower window shows that at $t = 10$ fm/c for the case without a first-order phase transition, when the density of the central cell is about 0.2 fm^{-3} in both cases. Although density

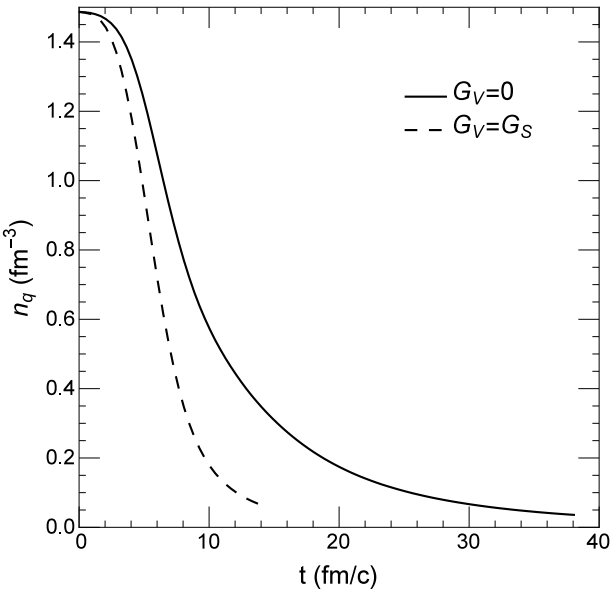

FIG. 10: Time evolution of the density of the central cell of an expanding quark matter obtained by averaging over 100 events for the two cases with (solid line) and without (dashed line) a first-order phase transition.

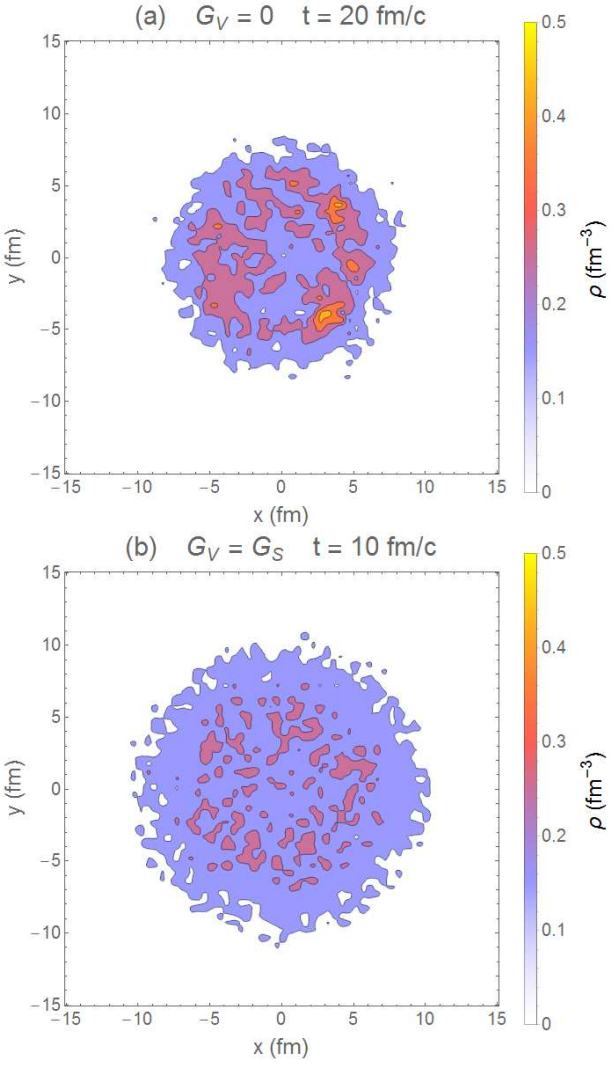

FIG. 11: (Color online). Density distributions of an expanding quark matter for a single event on the $z = 0$ plane at $t = 20$ fm/c for the case with a first-order phase transition (left window) and at $t = 10$ fm/c for the case without a first-order phase transition (right window).

clumps appear in both cases, those in the one with a first-order phase transition are significantly larger. As in the case of quark matter in a box, we can quantify the density fluctuations by the event-averaged scaled density moments [23]. They are shown in Fig. 12 by the black and red lines for the cases with and without a first-order phase transition, respectively. The dotted, dashed, and solid lines are for $N = 2$, 4, and 6, respectively. In both cases, the scaled density moments first increase and then decrease with time.This behavior is caused by the fast increase of the surface of the quark matter and the quick deviation from its initial smooth Wood-Saxon density distribution and the eventual decrease of the average density due to expansion. While the former leads to a broadened, density profile, which increases the volume of the low density regions and thus the scaled density moments, the latter shrinks the density profile and thus decreases the scaled density moments. Although the scaled density moments in the case without a first-order phase transition are larger than one, those in the case with a first-order phase transition are much larger, reflecting the effect due to density clumps that distribute randomly inside the expanding quark matter. However, previous studies have indicated that possible signals for the enhanced scaled density moments are strongly diluted in experimental observables [21].

Since density fluctuations can lead to spatial anisotropy even in central heavy ion collisions, it has been suggested that they may affect the anisotropic flows in the transverse plane [13, 14]. The latter are defined by the coefficients v_n in the expansion of the transverse momentum distribution $f(p_T, \phi)$ as a Fourier series in the azimuthal angle ϕ,

$$f(p_T, \phi) = \frac{N(p_T)}{2\pi}\{1 + 2\sum_{n=1}^{\infty} v_n(p_T)\cos[n(\phi - \psi_n)]\}, \quad (17)$$

where ψ_n is the event plane angle [24]. To calculate the anisotropic flow coefficients, we use the two particle cumulant method [25, 26], namely, $v_n\{2\} = \sqrt{\langle\cos(n\Delta\phi)\rangle}$ by averaging over all pairs of test particles in an event. We have calculated $v_2\{2\}$ and $v_4\{2\}$ for 100 events of an expanding quark matter with the same blast wave initial conditions, and their respective final event distributions are shown in the upper and lower windows of Fig. 13 with the solid and dashed lines for the cases with and without first order phase transition, respectively. Both

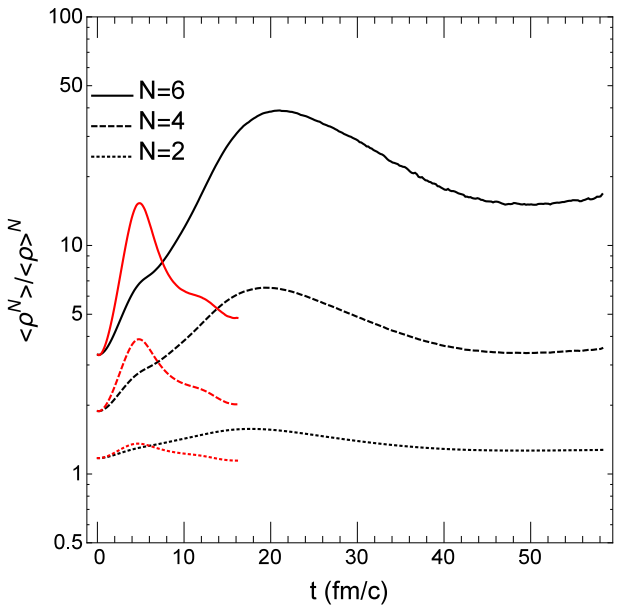

FIG. 12: (Color Online). Scaled density moments obtained by averaging over 100 events as functions of time for the cases with (black lines) and without (red lines) a first-order phase transition.

distributions peak at a larger value for the case with a first-order phase transition, particularly for v_4, thus providing a plausible signal for the first-oder phase transition. However, the values of the fluctuation induced v_2 and v_4 are much smaller than those in non-central heavy ion collisions.

We have also studied the effect of density fluctuations on dilepton production from a quark matter. Since the dilepton production rate is proportional to the square of parton density, more dileptons are produced when the density fluctuation is large. Also, a longer partonic phase as a result of a first-order phase transition would increase the depletion yield as well. As usually done in studying dilepton production in heavy ion collisions [27], we use the perturbative approach to calculate the dilepton yield from the quark-antiquark scattering by neglecting its effect on the dynamics of the expanding quark matter. Using the dilepton production cross section,

$$\sigma_{q\bar{q}\to e^+e^-} = \frac{4\pi\alpha^2}{3M^2}\sqrt{\frac{1-4m_e^2/M^2}{1-4m_q^2/M^2}} \times\left(1+2\frac{m_e^2+m_q^2}{M^2}+4\frac{m_e^2m_q^2}{M^4}\right), \quad (18)$$

where $M^2=(p_{e^-}+p_{e^+})^2$ is the square of the dilepton invariant mass, we have calculated the dilepton invariant mass spectrum by averaging over 100 events from the expanding quark matter, and they are shown in Fig. 14 by the solid and dashed lines for the cases with and without first-order phase transition, respectively. As expected, more dileptions are produced from the quark matter with

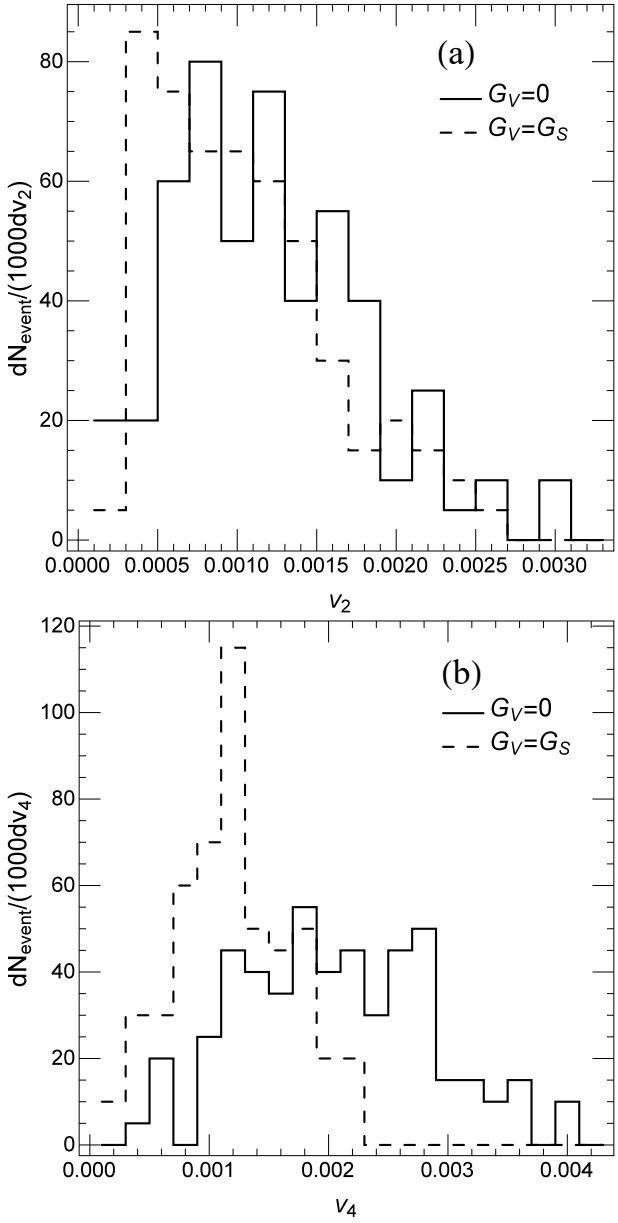

FIG. 13: Final anisotropic flow coefficients v_2 (upper window) and v_4 (lower window) distributions for 100 events of an expanding quark matter with the same blast wave initial conditions.

a first-order phase transition. We note the dilepton invariant mass spectrum peaks at $M\approx 0.5$ GeV with the peak value being about 3.5×10^{-4} GeV^{-1}, which is comparable with the result obtained from a hadronic transport model [28]. This enhancement in dilepton production may thus be detectable in experiments.

We note that like in other chiral quark models [14], quark matter in the NJL model can be bound at certain densities and temperatures. The region for such a unphysical state of matter is shown in Fig. 9 by the red color. Since the phase trajectory does not enter this region, the density fluctuations and their effects on

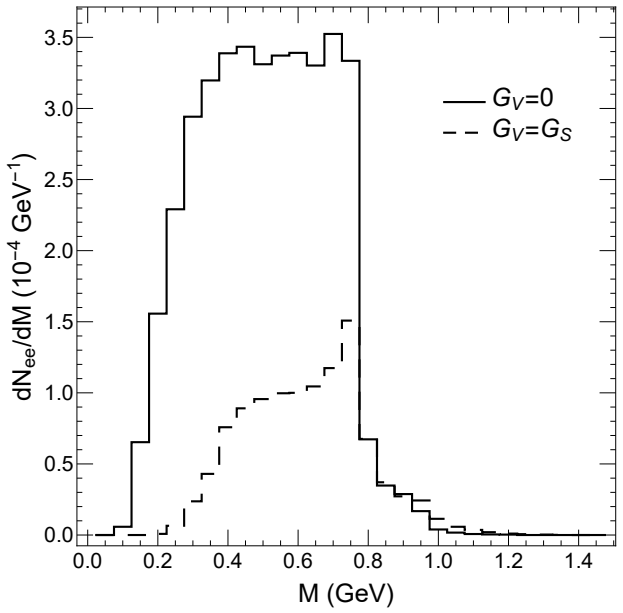

FIG. 14: Dilepton yield, averaged over 100 events, as a function of the invariant mass M for the cases with (solid line) and without (dashed line) a first-order phase transition in an expanding quark matter with the blast wave initial conditions.

anisotropic flows and dilepton production presented in the above are not due to the formation of stable quark droplets during the expansion of the quark matter.

B. AMPT initial conditions

In this subsection, we use a more realistic initial parton distribution for heavy ion collisions. Specifically, the initial partons are obtained from a multiphase transport (AMPT) model with string melting [29] that uses the heavy ion jet interaction generator (HIJING) [30–32] as the input. This model includes not only the minijet partons from initial hard collisions but also hadrons produced from excited strings, which are projectile and target nucleons that have suffered interactions, by converting them to partons according to the flavor and spin structures of their valence quarks. In particular, a meson is converted to a quark and an anti-quark, while a baryon is first converted to a quark and a diquark, and the diquark is then decomposed into two quarks. The quark masses are taken to be $m_u = 5.6$, $m_d = 9.9$, and $m_s = 199$ MeV/c^2 as in the PYTHIA program [33]. The above two-body decomposition is isotropic in the rest frame of the parent hadron or diquark. These partons are produced after a formation time of $t_f = E_H/m_{T,H}^2$, with E_H and $m_{T,H}$ denoting, respectively, the energy and transverse mass of the parent hadron. To obtain these partons as the initial conditions for our study of an expanding quark matter, we run the AMPT program with vanishing parton scattering cross sections in Zhang's parton cascade (ZPC)[34] and with the hadronic afterburner based on a relativistic transport (ART) [35, 36] turned off. In the AMPT, these partons are assumed to be produced at the tip of the light cone, i.e., on a thin disk perpendicular to the longitudinal axis or beam direction, which is reasonable in collisions at the top energy of RHIC. For collisions at lower energies such as in the BES experiments, the initial parton distribution is expected to be more extended in the longitudinal direction, and we take this into account by increasing the thickness of the initial disk to $2dm_N/\sqrt{s_{NN}}$ for head-on collisions, where d is the diameter of the colliding nuclei, and assuming that the initial partons are uniformly distributed in this disk.

Using 1000 test partons for each physical partons produced from Au+Au collisions at zero impact parameter and a center-of-mass energy $\sqrt{s_{NN}} = 2.5$ GeV and smearing the distribution of initial partons from the AMPT with a longitudinal length of $d/3.5$ to mimic the initial conditions for collisions at $\sqrt{s_{NN}} = 7$ GeV, we have found that some parts of the system go through the spinodal region when the SU(3) NJL model with $G_V = 0$ is used in the Boltzmann equation and in constructing the phase diagram.

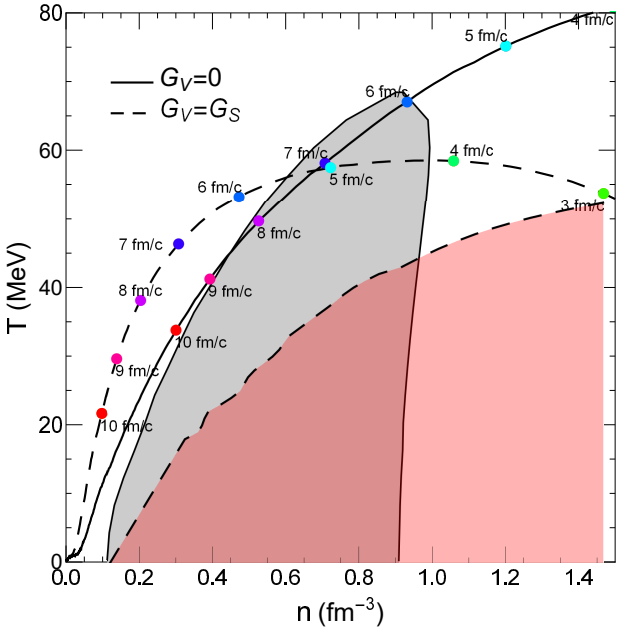

FIG. 15: (Color online). Same as Fig. 9 for the phase trajectories of the central part of an expanding quark matter obtained by averaging over 100 events for the cases with (solid line) and without (dashed line) a first-order phase transition using the initial parton distribution from the AMPT model that is smeared in the longitudinal direction as described in the text.

As shown by the solid line in Fig. 15, the trajectory of the central part of the system, obtained by averaging over 100 events for the case with a first-order phase transition, goes into the spinodal instability region at about 6 fm/c after expansion, and moves out of this region at about

8.5 fm/c. As in the case of blast-wave initial conditions, the phase trajectory of the expanding quark matter never enters the region where stable quark droplets exist. Although 2.5 fm/c is too short for the spinodal instability to develop in the central part of the quark matter, its other parts may stay longer in the spinodal instability region as shown below. For the case without a first-order phase transition, the trajectory is shown by the dashed line in Fig. 15. We note that the initial temperatures in these two cases are different, since the temperature in the $G_V = G_S$ case is lower than that in the $G_V = 0$ case for the same parton distribution.

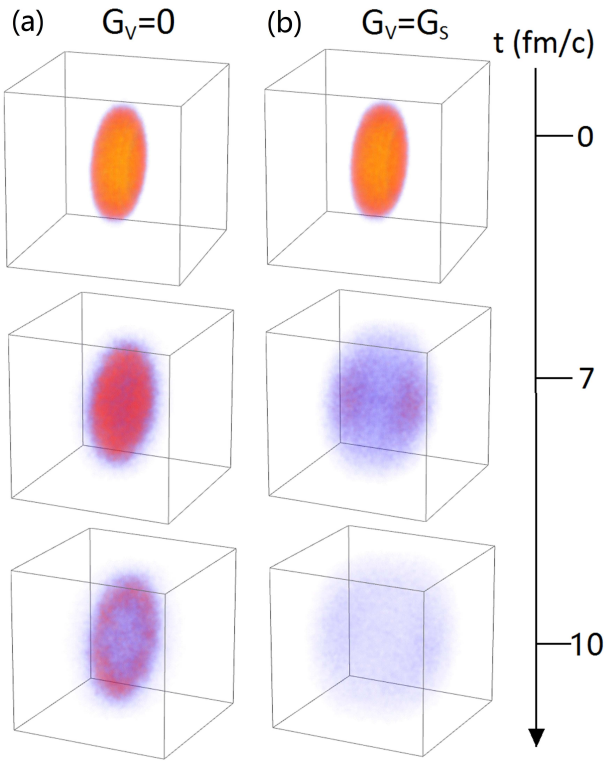

FIG. 16: (Color online). Time evolution of the density distributions in a single event in central Au+Au collisions at $\sqrt{s_{NN}} = 2.5$ GeV using smeared initial conditions from the AMPT for the cases with (left column) and without (right column) a first-order phase transition.

A 3-dimensional view of the time evolution of the density distributions in a single event using the same AMPT initial conditions but two different equations of states with (left column) and without (right column) a first-order phase transition is shown in Fig. 16, where high and low densities are depicted in orange and blue colors, respectively. In the case with a first-order phase transition, i.e. G_V is set to zero, a disk of high density appears due to its lower pressure as a result of the spinodal instability, which later transforms into several disjointed clusters on a ring at $z = 0$. These cold and dense clusters stay in the spinodal instability region even at $t = 14$ fm/c, which agrees with the statement in the previous paragraph. The dynamics in the case without

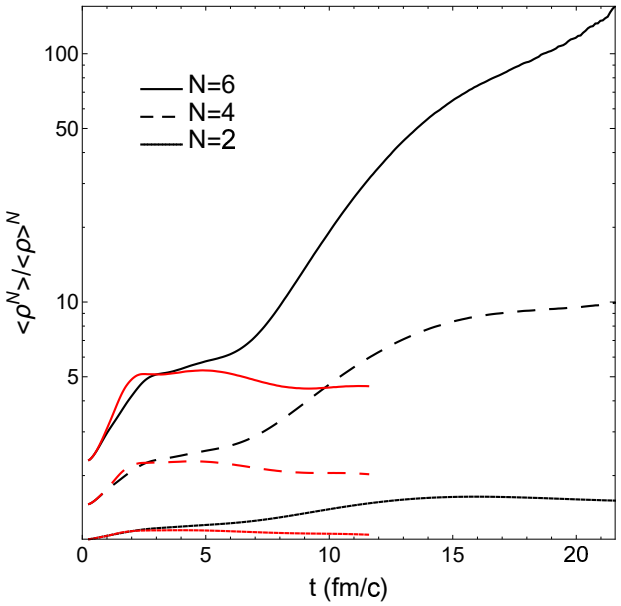

FIG. 17: (Color Online). Scaled density moments averaged over 100 events as functions of time for the cases with (black lines) and without (red lines) a first-order phase transition.

a first-order phase transition is, on the other hand, quite different. Due to the large pressure gradient in the longitudinal direction, the system first expands along this direction and form two high density regions at the two ends. After further expansion when the two dense regions disappears, the whole system becomes a uniform and dilute gas at $t \approx 10$ fm/c. It is further seen from Fig 16 that the quark matter with a first-order phase transition expands slower than that without a first-order phase transition.

The dense clumps or density fluctuations shown in the left column of Fig. 16 can again be quantified by the event-averaged scaled density moments as shown in Fig. 17 for the 2nd (dotted curve), 4th (dashed curve), and 6th (solid curve) order scaled moments with the black and red colors denoting results obtained with and without a first-order phase transition, respectively. It is seen that the density moments continue to increase during the spinodal tdecomposition or first-order transition, which is different from the cases with a spherical initial distributions in the previous section, and saturate at higher values than in the case without a first-order phase transition. Such a feature is more prominent for the higher-order scaled density moments.

The dense clumps on the $z = 0$ plane in Fig. 16 also affect the final rapidity distribution of quarks by slowing down the expansion in the longitudinal direction, thus reducing their rapidities to a narrow region around the mid-rapidity. As shown by the solid line in the upper window of Fig. 18, the event averaged parton rapidity distribution in the case with a first-order phase transition is much narrower than that in the case without a first-order phase transition shown by the dashed line.

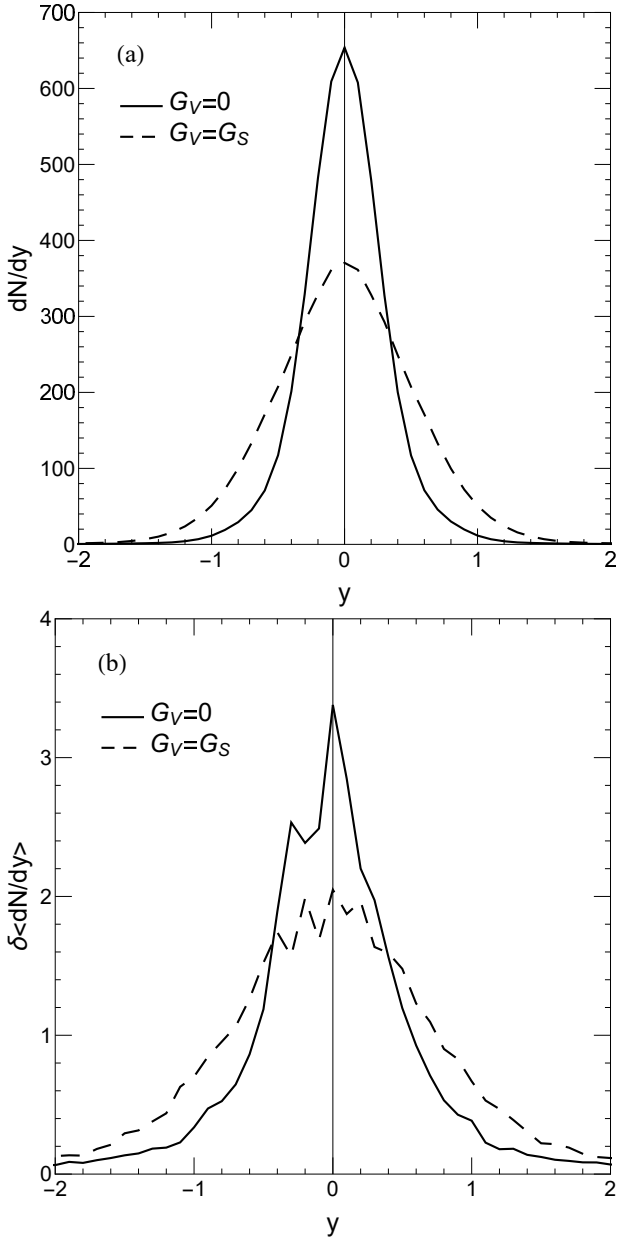

FIG. 18: Final rapidity distribution of quarks averaged over 100 events (upper window) and its event-by-event variance (lower window) for the cases with (solid curve) and without (dashed curve) a first-order phase transition from an expanding quark matter using the AMPT initial conditions.

The event-by-event fluctuation of the quark number in each rapidity bin, which is shown in the lower window of Fig. 18, is also enhanced in the small rapidity region by the first order-phase transition. This effect can be regarded as a possible signal of a first-order phase transition and is worth studying in experiments.

We have also studied the event averaged dilepton invariant mass spectrum from an expanding quark matter with initial conditions from the AMPT model. This is shown in Fig. 19 by the solid and dashed lines for

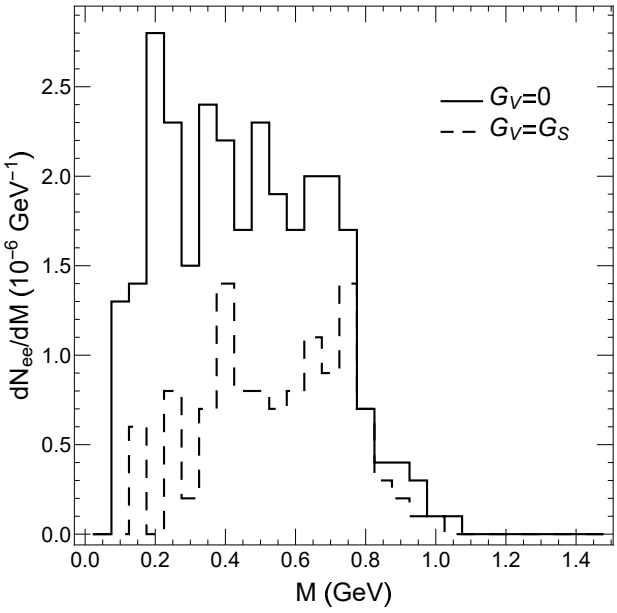

FIG. 19: Dilepton yield averaged over 100 events as a function of invariant mass $\sqrt{s}$ for the cases with (solid curve) and without (dashed curve) a first-order phase transition from an expanding quark matter using the AMPT initial conditions.

the cases with and without a first-order phase transition, respectively. As in the previous section using the blast-wave initial conditions, the presence of a first-order phase transition enhances the dilepton yield as a result of density fluctuations and a longer partonic phase. However, the dilepton yield is lower than that obtained from the calculation with the blast wave initial condition by two orders of magnitude because there are very few antiquarks in the partonic matter produced in heavy ion collisions at the low collision energy considered here and also because we have not included the bremsstrahlung contribution to dilepton production from the quark-quark scattering.

V. CONCLUSIONS

The spinodal instability is a thermodynamic feature of a first-order phase transition in a many-body system. It occurs when its pressure in some parts decreases with increasing density. This can amplify the density fluctuations and lead to a phase separation in the system. We have studied this phenomenon by solving the Boltzmann equations using the test particle method. The calculations are based on the NJL model, which has been shown to give good a description of the vacuum properties of the hadrons and also predicts the existence of a first-order phase transition in baryon-rich quark matter. We have obtained some intuitive pictures on the phase separation in a quark matter that is either in a static box or undergoes expansion. For the case of a static box, we have found that the growth rates extracted from the

early growth of a sinusoidal density fluctuation agree with the analytical results obtained from the linearized Boltzmann equation. We have also calculated the higher-order density moments of the quark matter and found them to increase and saturate at large values after phase separation. The skewness of the quark number event-by-event distribution in a small sub-volume of the quark matter is also found to increase, but this feature disappears if the sub-volume is large. As for the expanding quark matter, two cases have been studied. One is based on the blast-wave initial conditions, while the other uses the AMPT initial conditions. In both cases, we have found that the expansion of the quark matter is slowed down by the presence of a first-order phase transition. Density clumps are found to appear and lead to an anisotropy in the momentum space, which can be characterized by the scaled density moments and the anisotropic flows v_2 and v_4, respectively. An enhancement in the dilepton yield is also observed. The expansion of the quark matter with the AMPT initial conditions is more complex. The dense clumps are mostly formed on the middle transverse plane, resulting in a narrower rapidity distribution.

In the future, we plan to develop a more consistent transport model, in which all cross sections are calculated self-consistently from the NJL model, so that the temperature and density dependence of the collisional effect can be taken into account. The dilepton production through the $qq \to qqe^+e^-$ process will also be included, since it could be the main contribution to the dilepton yield from a quark matter of high baryon chemical potential. We also plan to extend the transport model using the PNJL model [37], which is more realistic and agrees better with the lattice results for the properties of quark matter with low baryon chemical potential. We hope that our study will help to understand the phase transition in the baryon-rich matter by comparing theoretical predictions with available and future experimental data.

Acknowledgements

This work was supported by the US Department of Energy under Contract No. DE-SC0015266 and the Welch Foundation under Grant No. A-1358.

Appendix: Finite grid size effects

Counting partons in a grid of finite size in evaluating the mean fields effectively allows the partons in the grid interact with each other, thus modifying the contact interactions in the NJL model to finite-range ones. To study this effect, we need to calculate the probability for two partons in the same grid to have a separation $\Delta\mathbf{x}$. Given a parton located at $x \in [0, a]$ in a 1-dimensional grid $[0, a]$, the probability to find another parton located at $x + \Delta x$ in the same grid is

$$\begin{aligned} P(\Delta x) &= \frac{1}{a}\int dx\theta(x)\theta(a-x)\theta(x+\Delta x)\theta(a-x-\Delta x) \\ &= \mathrm{tri}\left(\frac{\Delta x}{a}\right), \end{aligned} \tag{A.1}$$

where

$$\mathrm{tri}(x) \triangleq \max(0, 1-|x|). \tag{A.2}$$

The above expression can be straightforwardly generalized to the 3-dimensional case to give

$$P(\Delta\mathbf{x}) = \prod_i \mathrm{tri}\left(\frac{\Delta x^i}{a^i}\right), \tag{A.3}$$

where $\{a^1, a^2, a^3\}$ are the grid lengths. The interaction between two partons at $\mathbf{x}$ and $\mathbf{y}$ is then replaced by

$$\begin{aligned} G_S\delta^3(\mathbf{x}-\mathbf{y}) &\to \frac{G_S}{\prod_i a^i}\prod_i \mathrm{tri}\left(\frac{x^i-y^i}{a_i}\right), \\ K\delta^3(\mathbf{x}-\mathbf{y}) &\to \frac{K}{\prod_i a^i}\prod_i \mathrm{tri}\left(\frac{x^i-y^i}{a_i}\right). \end{aligned} \tag{A.4}$$

Transforming Eq. (A.4) from $\mathbf{x}$-space to $\mathbf{k}$-space gives

$$\begin{aligned} G_S \to \tilde{G}_S &= G_S\prod_i \frac{2\cos(a^ik_i)-2}{a^ik_i}, \\ K \to \tilde{K} &= K\prod_i \frac{2\cos(a^ik_i)-2}{a^ik_i}. \end{aligned} \tag{A.5}$$

Note that in the limit that $a^ik_i \to 0$ for all i, $\tilde{G}_S \to G_S$ and $\tilde{K} \to K$, which means the modification does not affect the long wavelength modes.

Replacing G_S and K in Eq. (35) in Ref. [6] with $\tilde{G}_S$ and $\tilde{K}$, respectively, and solving the resulting equation, we obtain the modified dispersion relation, and they are shown in Fig. 2 for a grid size $a^i = 2/3$ fm by the solid and dashed lines for the cases with and without the collision term, respectively. As expected, the growth rate Γ_k is not much affected in the small k region but is significantly suppressed in the large k region. The finite grid size effect is thus similar to the quantum effect shown in Ref. [6]. Using a finite grid size essentially allows partons to interact at finite separation, resulting in an effective finite-range interaction. This effect can be corrected by reducing the size of the grid.

[1] T. K. Nayak (STAR Collaboration), Nucl. Phys. A **830**, 555C (2009).

[2] M. M. Aggarwal et al. (STAR), Phys. Rev. Lett. **105**,

022302 (2010).
[3] D. McDonald (STAR), EPJ Web Conf. **95**, 01009 (2015).
[4] L. Adamczyk et al. (STAR), Phys. Rev. Lett. **112**, 032302 (2014).
[5] L. Adamczyk et al. (STAR), Phys. Rev. Lett. **113**, 092301 (2014).
[6] F. Li and C. M. Ko, Phys. Rev. C **93**, 035205 (2016).
[7] S. P. Klevansky, A. Ogura, and J. Hufner, Ann. Phys. **261**, 37 (1997).
[8] R. Marty and J. Aichelin, Phys. Rev. **C87**, 034912 (2013).
[9] R. Marty, J. M. Torres-Rincon, E. Bratkovskaya, and J. Aichelin, J. Phys. Conf. Ser. **668**, 012001 (2016).
[10] O. Scavenius, A. Dumitru, E. S. Fraga, J. T. Lenaghan, and A. D. Jackson, Phys. Rev. **D63**, 116003 (2001).
[11] J. Steinheimer and J. Randrup, Phys. Rev. Lett. **109**, 212301 (2012).
[12] C. Herold, M. Nahrgang, I. Mishustin, and M. Bleicher, Nucl. Phys. A **925**, 14 (2014), ISSN 0375-9474.
[13] C. Herold, M. Nahrgang, I. Mishustin, and M. Bleicher, J. Phys. Conf. Ser. **509**, 012065 (2014).
[14] J. Steinheimer, J. Randrup, and V. Koch, Phys. Rev. C **89**, 034901 (2014).
[15] N. M. Bratovic, T. Hatsuda, and W. Weise, Phys. Lett. B **719**, 131 (2013).
[16] G. 't Hooft, Phys. Rev. D **14**, 3432 (1976).
[17] M. Buballa, Phys. Rept. **407**, 205 (2005).
[18] B. R. Holstein, Phys. Lett. B **244**, 83 (1990).
[19] C.-Y. Wong, Phys. Rev. C **25**, 1460 (1982).
[20] G. F. Bertsch and S. Das Gupta, Phys. Rept. **160**, 189 (1988).
[21] J. Steinheimer and J. Randrup, Phys. Rev. C **87**, 054903 (2013).
[22] M. A. Stephanov, Phys. Rev. Lett. **102**, 032301 (2009).
[23] J. Randrup, Phys. Rev. C **82**, 034902 (2010).
[24] B. H. Alver, C. Gombeaud, M. Luzum, and J.-Y. Ollitrault, Phys. Rev. C **82**, 034913 (2010).
[25] S. Wang, Y. Z. Jiang, Y. M. Liu, D. Keane, D. Beavis, S. Y. Chu, S. Y. Fung, M. Vient, C. Hartnack, and H. Stöcker, Phys. Rev. C **44**, 1091 (1991).
[26] N. Borghini, P. M. Dinh, and J.-Y. Ollitrault, Phys. Rev. C **64**, 054901 (2001).
[27] L. Xiong, Z. G. Wu, C. M. Ko, and J. Q. Wu, Nucl. Phys. **A512**, 772 (1990).
[28] T. Galatyuk, P. M. Hohler, R. Rapp, F. Seck, and J. Stroth, Eur. Phys. J. **A52**, 131 (2016).
[29] Z.-W. Lin, C. M. Ko, B.-A. Li, B. Zhang, and S. Pal, Phys. Rev. C **72**, 064901 (2005).
[30] X.-N. Wang, Phys. Rev. D **43**, 104 (1991).
[31] X.-N. Wang and M. Gyulassy, Phys. Rev. D **44**, 3501 (1991).
[32] M. Gyulassy and X.-N. Wang, Comput. Phys. Commun. **83**, 307 (1994), ISSN 0010-4655.
[33] T. Sjstrand, Comput. Phys. Commun. **82**, 74 (1994), ISSN 0010-4655.
[34] B. Zhang, Comput. Phys. Commun. **109**, 193 (1998), ISSN 0010-4655.
[35] B.-A. Li and C. M. Ko, Phys. Rev. C **52**, 2037 (1995).
[36] B.-A. LI, A. T. Sustich, B. Zhang, and C. M. Ko, Int. J. Mod. Phys. E **10**, 267 (2001).
[37] K. Fukushima, Phys. Rev. D **77**, 114028 (2008), [Erratum: Phys. Rev. D 78, 039902(2008)].